# Dynamic Fracture of Nonglassy Suspensions

Matthieu Roché,[1] Eglind Myftiu,[1] Mitchell C. Johnston,[1] Pilnam Kim,[2] and Howard A. Stone[1]
[1]Department of Mechanical and Aerospace Engineering, Princeton University, Princeton, New Jersey 08544, USA
[2]Department of Bio and Brain Engineering, KAIST, Daejeon 305-701, Republic of Korea
(Received 17 October 2012; published 4 April 2013)

We study the dynamic fracture of thin layers of suspensions of non-Brownian rigid particles. The impact of a projectile triggers a liquid-to-solid transition and a hole opens in the layer. We show that the occurrence of fracture and the spatial and dynamic features of the cracks depend mostly on the thickness of the layer and the particle volume fraction. In contrast, the properties of the fractured material seem independent of volume fraction. Finally, we measure the velocity of the crack tip, from which we estimate an effective value of the shear modulus of the fractured material.

DOI: 10.1103/PhysRevLett.110.148304 PACS numbers: 83.80.Hj, 47.50.Gj, 62.20.M−, 83.60.Uv

A solid responds to stress in a different way than does a fluid: a simple solid will deform by a finite amount under a constant stress while a simple fluid will deform continuously. Despite this fundamental difference, both condensed states of matter will fracture if the applied stress becomes too high: cracks will grow in solid materials [1,2] whereas cavitation bubbles will appear in liquids [3,4].

Most real materials are neither ideal liquids nor ideal solids. Their response to stress depends on the rate at which they are deformed [5]. These complex materials also experience fracture. For example, polymer liquids [6–8], bridged emulsions [9,10], micellar fluids [11], and suspensions of hard particles [12–16] can fail under various conditions. The latter systems have attracted significant attention recently since the physics supporting their elastic response and their failure under large stresses is still poorly understood.

The response of suspensions of rigid particles is solidlike in at least two cases. In the first situation, a suspension at equilibrium reaches a glassy state when its particle volume fraction is increased above a critical value $\phi_g$ [17]. An example of the second situation, far from equilibrium, is shear thickening, which has been related to a dynamic jamming transition [18,19], resulting from a difference in the relative motions of the particles and the solvent [20]. Particle rearrangement and accompanying solidification occur also under pure extension and compression. As a result, threads of suspensions can buckle [16,21], and layers of suspension rigidify after an impact [22]. Fracture was reported both in extension [15,16] and in shear [23], but not characterized.

Here we document the dynamic fracture of thin layers of suspensions of non-Brownian particles that experience an impact. These suspensions have a small yield stress and shear thicken continuously. We characterize fracture by quantifying the spatial and dynamic properties of the crack pattern as well as crack propagation as a function of the energy delivered by the projectile and the properties of the layer of suspension. We show that the number of cracks per impact and their length depend mostly on the thickness of the layer and on the particle volume fraction. From a study of the conditions under which cracks nucleate and the velocity at which cracks propagate, we extract insights on the nature of the transient material formed by suspensions under large stresses.

For each experiment, a cylindrical metal rod (radius $a = 6.7 \times 10^{-3}$ m, length $L_r = 0.127$ m) was released through a guide from a height $10^{-2}$ m $\leq H \leq 1$ m onto the surface of a layer of suspension [see Fig. 1(a)]. The square layer ($L_s = 14 \times 10^{-2}$ m) had a thickness $5 \times 10^{-3}$ m $\leq h \leq 35 \times 10^{-3}$ m and rested on a substrate made of steel (thickness $w_s = 12.5 \times 10^{-3}$ m) or plexiglas ($w_s = 51 \times 10^{-3}$ m, used to record views from below the layer). After each experiment, we checked that the substrate remained undamaged. High-speed cameras (Vision Research Phantom v7.3 and v9.1) recorded impact events at rates between 1000 and 20 000 frames per second.

We used aqueous suspensions of corn starch (CS; Sigma-Aldrich, density $\rho \simeq 1590$ kg m$^{-3}$). Until dispersion, corn starch was stored in a humidity-controlled vacuum chamber to minimize moisture contamination. Before each experiment, we dispersed the particles (average diameter $\bar{d} \simeq 15$ $\mu$m) in a density-matched aqueous solution of cesium chloride (CsCl, [CsCl] = 55 wt%) [24]. The particle volume fraction was in the range $0.37 \leq [\mathrm{CS}] \leq 0.42$. Higher volume fractions proved difficult to handle. These suspensions had a yield stress in shear $\sigma_c \leq 1$ Pa (see Fig. S1 in the Supplemental Material [25]). For stresses $\sigma > \sigma_c$, the shear viscosity of the suspensions first decreased as the shear stress increased, and increased continuously above a critical shear stress. To begin an experiment, the suspension was poured in the container and allowed to relax for a few minutes before impact events were recorded. We prepared a new layer every 20 minutes to minimize the effect of evaporation.

Using a tungsten carbide rod (density $\rho_r = 15\,800$ kg m$^{-3}$, mass $m_r = (303 \pm 1) \times 10^{-3}$ kg), we observed cracks for suspensions with volume fractions $[\mathrm{CS}] \geq 0.39$. A top-view image sequence (see Fig. 1(b)

 

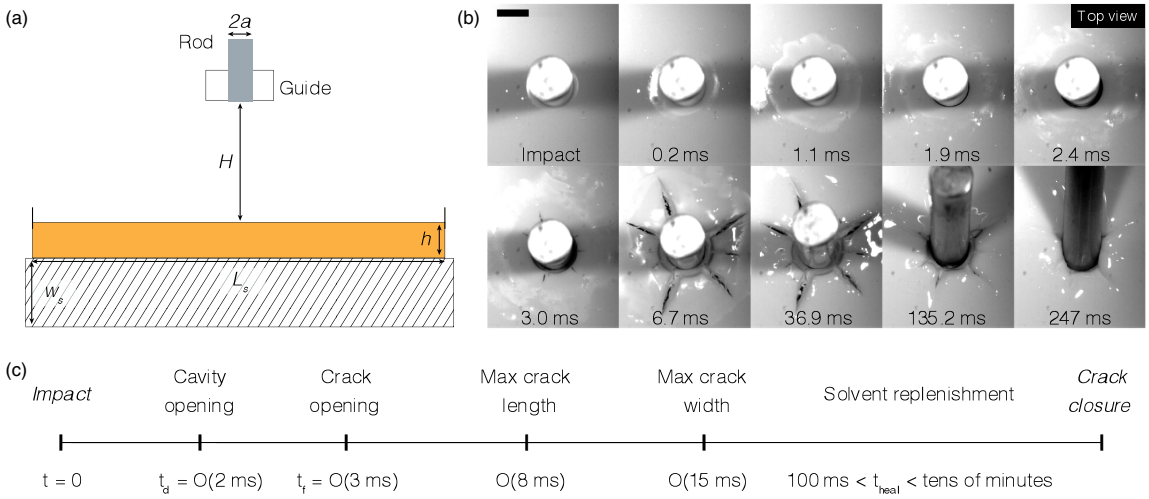


FIG. 1 (color online). (a) Schematic of the experimental set-up. (b) Time sequence, extracted from a top view of a layer of corn starch suspension ([CS] = 0.40), after the impact of a tungsten carbide rod. $H = (77 \pm 1) \times 10^{-2}$ m, $h = (1 \pm 0.1) \times 10^{-2}$ m. Scale bar: $10^{-2}$ m. (c) Timeline of fracture after impact, with definitions of the time at which the hole detached from the surface of the rod $t_d$ and the time at which fracture initiated $t_f$.

and movie M1 in the Supplemental Material [25]) shows that a wave propagated across the surface of the layer just after impact ($t = 0$ to $1.1 \times 10^{-3}$ s). Then, a hole opened around the rod ($t = 1.9 \times 10^{-3}$ s) in an area where the texture of the suspension had changed from glossy to matt. We associate this change of texture to an impact-induced solidification of suspensions that was identified recently [22] in layers thicker and with higher initial particle volume fractions than the layers we used here.

Cracks appeared on the contour of the hole [see Fig. 1(b), $t = 3.0 \times 10^{-3}$ s]. The cracks opened in the plane of the layer of the suspension, as in mode-1 fracture [1]. These crack patterns were similar to those observed after the impact of nondeformable projectiles on brittle materials [26,27]. Simultaneous top and bottom views of the set-up (see movie M2 in the Supplemental Material [25]) show that the formation of cracks occurred during the penetration of the rod, before the rod reached the bottom of the layer and the surface of the substrate. The angle at the tip of the cracks was on the order of 10 deg. Cracks propagated along straight trajectories until they reached their maximum extension $L_c$ [see Fig. 1(b), $t = 6.7 \times 10^{-3}$ s]. The same picture indicates that the suspension yielded under shear in the plane of the layer, in a fashion similar to plastic deformation (see Fig. S2 in the Supplemental Material [25]). Crack extension was limited by the size of the drier area, which depended weakly on the potential energy $E_p = m_r g H$, with $g$ the acceleration of gravity (see Fig. S3 in the Supplemental Material [25]), and the cracks that nucleated first were longer than cracks appearing later. Then cracks widened until their contours became blunt and glossy. Eventually, the solvent returned towards the fractured region [see Fig. 1(b), $t = 36.9 - 247 \times 10^{-3}$ s]. Recovery took a few hundred milliseconds, but structures similar to aggregates obtained by granulation [14] with relaxation time scales of several tens of minutes were observed after impact for the most concentrated suspensions ([CS] = 0.42). We prepared a new layer every time these structures were observed. Figure 1(c) summarizes the time sequence of fracture.

Fracture is one way for the stressed material to dissipate the potential energy $E_p$ that the projectile delivers at impact. Therefore, the properties of the crack pattern are likely to depend on $E_p$. As a preliminary test, we measured the probability density function (PDF) of the number of cracks $N_c$ per impact obtained for fixed $H$, $h$, and [CS] [see Fig. 2(a)]. The PDF is peaked around a well defined value, in a fashion similar to the PDF reported for thin, initially crack-free, sheets of aluminum [28]. Therefore the reproducibility of the properties of the crack pattern at a given potential energy $E_p$ is good.

Taking into account the PDF of $N_c$, we investigated the relation between the crack pattern and both the release height $H$ and the particle volume fraction [CS] for a constant thickness $h$. Figure 2(b) shows that the average number of cracks per impact $\bar{N}_c$ increases as $H$ is increased to reach a plateau value above $H \simeq 0.5$ m. For a given $H$, $\bar{N}_c$ does not depend on [CS]. In Fig. 2(c), the average length of cracks per impact $\bar{L}_c$ is seen to depend on $H$ in a fashion qualitatively similar to $\bar{N}_c$. From Figs. 2(b) and 2(c) and by changing the density of the rod ($2\,700\ \mathrm{kg\,m^{-3}} < \rho_r < 15\,800\ \mathrm{kg\,m^{-3}}$), we estimated that the potential energy $E_f = E_{p,\mathrm{crack}}$ required to trigger fracture was $E_f \simeq 0.1$ J. We could not estimate the critical stress at fracture as it depended on energy dissipation during the penetration of the rod before fracture, which was difficult to quantify.

Crack propagation in solids is known to depend on the thickness of the sample [29]. For $0.39 \leq [\mathrm{CS}] \leq 0.42$, we observed cracks when the thickness $h$ was below a critical value $h_c \leq 2 \times 10^{-2}$ m [see Fig. 2(d)]. The average

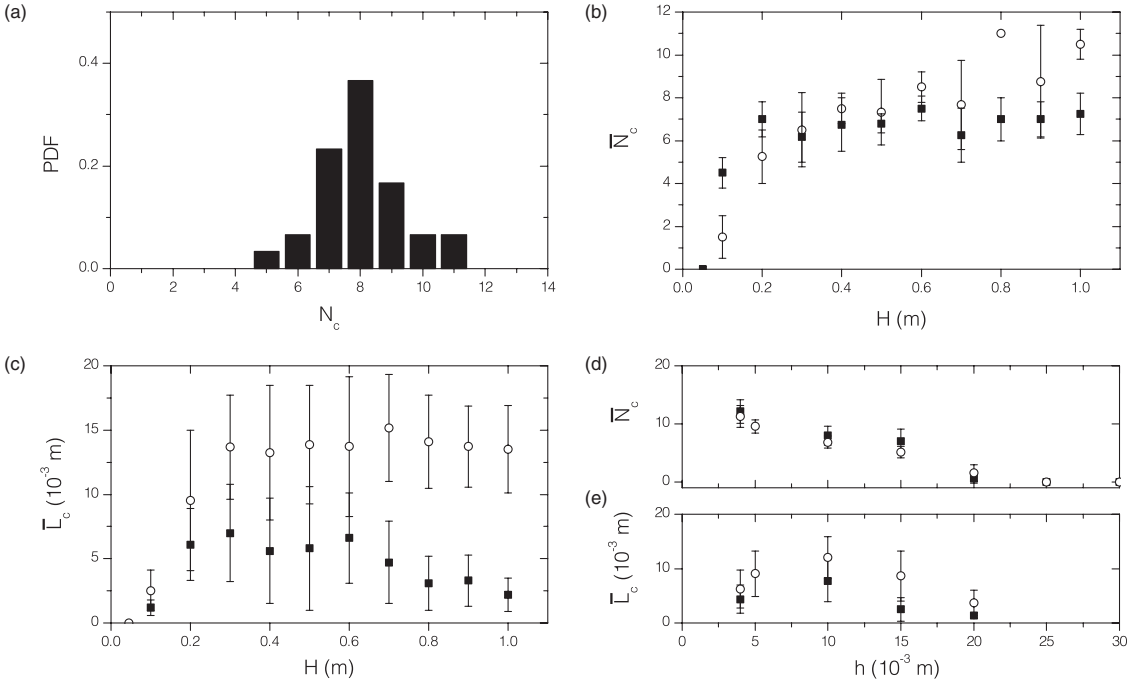


FIG. 2. (a) Normalized probability density function (PDF) of the number of cracks $N_c$. The plot summarizes 30 experiments. [CS] = 0.42, $h = (1 \pm 0.1) \times 10^{-2}$ m, $H = (77 \pm 1) \times 10^{-2}$ m. (b) The average number of cracks $\bar{N}_c$ and (c) the average crack length $\bar{L}_c$ per impact as a function of the release height $H$. $h = (1 \pm 0.1) \times 10^{-2}$ m, [CS] = 0.40 (filled square) and [CS] = 0.42 (open circles). (d) Average number of cracks $\bar{N}_c$ and (e) average crack length $\bar{L}_c$ (bottom) per impact as a function of the thickness $h$ of the layer. [CS] = 0.40 (filled square) and 0.42 (open circles); $H = (77 \pm 1) \times 10^{-2}$ m.

number of cracks per impact $\bar{N}_c$ appeared to be inversely proportional to $h$ while being independent of [CS]. The average crack length $\bar{L}_c$ also increased as $h$ decreased [see Fig. 2(e)]. These observations are a consequence of the finite rate of solidification of layers of suspension experiencing an impact [22]: the time to solidify a layer across its entire thickness decreases as the thickness decreases. Hence, for a given particle volume fraction, a decrease of the thickness of the layer increases the amount of energy remaining to be released after solidification. This observation establishes the thickness as a critical parameter to understand fracture in suspensions.

We observed a decrease in the average length of the cracks $\bar{L}_c$ for both release heights $H > 0.6$ m [see Fig. 2(c)], i.e., increasing potential energies $E_p$, and for thicknesses $h < 10 \times 10^{-3}$ m [see Fig. 2(e)]. In these experiments, the cylinder touched the top surface of the substrate and bounced back, dissipating part of the energy in the supporting plate. Moreover, in contrast to $\bar{N}_c$, both the studies with release height $H$ and layer thickness $h$ showed that the average crack length $\bar{L}_c$ increased with [CS]. We interpret the relation between $\bar{L}_c$ and [CS] as follows. For a given particle size, layer thickness, and release height, increasing the particle volume fraction (i.e., decreasing the interparticle distance) leads to faster solidification of the suspension [22]. As the particle volume fraction increases, more energy remains to be dissipated after solidification, resulting in the increase of $\bar{L}_c$ with [CS]. We also tested the influence of the size of the projectile and its shape. We observed that an increase of the size of the projectile led to an increase in $\overline{N}_c$ while $\overline{L}_c$ did not vary (see Fig. S4 in the Supplemental Material [25]). We note that the geometry of the crack pattern depends on the shape of the projectile (see Fig. S5 in the Supplemental Material [25]).

The importance of the different processes underlying energy dissipation in the suspension can be deduced from the results presented in Fig. 2 and the previous discussion. We compare the capillary surface energy $E_s$ required to open the cracks to $E_f$. The opening of one crack created two interfaces with air. For this discussion, we estimate $E_s$ for a $10^{-2}$-m thick layer with a volume fraction [CS] = 0.42, for which $\bar{N}_c = 8$ and $\bar{L}_c = 12 \times 10^{-3}$ m [see Fig. 2(e)]. For all of the suspensions, this estimate captured the order of magnitude of $E_s$, which is given by

$$E_s = 2\bar{N}_c \bar{L}_c h \gamma, \tag{1}$$

where $\gamma$ is the interfacial tension between air and the suspension that we had measured previously [21], $\gamma \simeq 73 \times 10^{-3}$ N m$^{-1}$. Hence, we find $E_s \simeq 1.4 \times 10^{-4}$ J, which is 3 orders of magnitude smaller than the threshold potential energy $E_f \simeq 0.1$ J. Therefore most of the energy delivered by the projectile was transformed through processes such as viscous dissipation, solidification, and elastic energy during both the penetration of the rod in the suspension and crack opening.

Now we characterize the conditions for crack nucleation with a study of the dynamics of the hole that opened around the cylinder between impact and fracture [see Fig. 1(b),

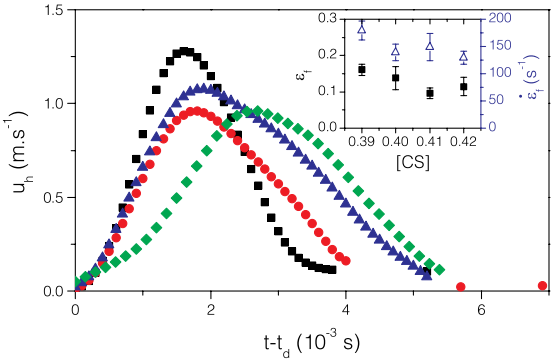


FIG. 3 (color online). (a) Velocity of the hole contour $u_h$ as a function of time $t - t_d$, with $t_d$ the time at which the hole detaches from the rod, for volume fractions [CS] = 0.39 black square, 0.40 red circle, 0.41 green diamond and 0.42 blue triangle. Inset: Ultimate strain $\epsilon_f$ black square and ultimate strain rate $\dot{\epsilon}_f$ open triangle at which cracks nucleated on the contour as a function of [CS]. $H = (40 \pm 1) \times 10^{-2}$ m, $h = 15 \times 10^{-3}$ m.

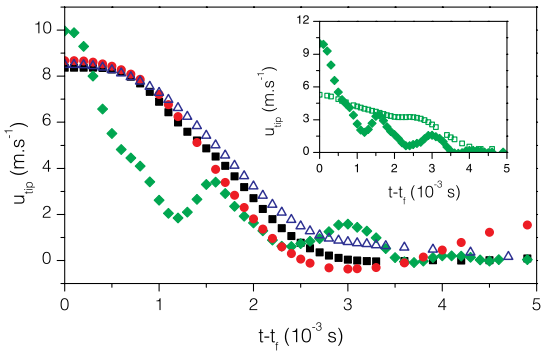


FIG. 4 (color online). Velocity of the tip of the crack $u_{\text{tip}}$ as a function of time for [CS] = 0.4 (open triangle, $h = 10 \times 10^{-3}$ m) and 0.42 (black square $h = 5 \times 10^{-3}$ m, red circle $h = 10 \times 10^{-3}$ m, green diamond $h = 15 \times 10^{-3}$ m). $H = (77 \pm 1) \times 10^{-2}$ m. Inset: Crack tip velocity for two first cracks created by impact from different heights. [CS] = 0.42, $h = 15 \times 10^{-3}$ m, open square $H = (20 \pm 1) \times 10^{-2}$ m and green diamond $H = (77 \pm 1) \times 10^{-2}$ m.

$1.1\,\text{s} \leq t \leq 2.4 \times 10^{-3}\,\text{s}$]. Using custom MATLAB code [30] to compute the first derivative of spline fits to the trajectory of the hole contour $r_h(t)$ (see Fig. S6 in the Supplemental Material [25]), we observed that the velocity $u_h$ of the contour increased just after detachment (see Fig. 3). The time at which $u_h$ peaked, at a magnitude on the order of $1\,\text{m}\,\text{s}^{-1}$, corresponded to the crack opening time $t_f$. The maximum speed did not appear to depend significantly on the particle volume fraction. Then the contour slowed down, and stopped well before the cracks reached their maximum length [$t \simeq 8 \times 10^{-3}$ s, see Fig 1(b)].

The opening of the hole induced a tensile strain on the suspension in the vicinity of the cavity. From the opening dynamics, we measured the ultimate strain $\epsilon_f = \frac{r_h(t=t_f)-a}{a}$ and the ultimate strain rate $\dot{\epsilon}_f = \frac{1}{r_h}\frac{dr_h}{dt}$ at the time $t_f$ at which fracture occurred (see the inset in Fig. 3). Cracks opened when $\epsilon_f \simeq 0.12$, a value which is comparable to the ultimate strain measured before fracture was observed in a study of similar suspensions under extension [15]. We measured ultimate strain rates $\dot{\epsilon}_f \simeq 150\ \text{s}^{-1}$, which are much higher than the value reported for strain hardening to happen, $\dot{\epsilon} > 0.3\ \text{s}^{-1}$ [15]. Both $\epsilon_f$ and $\dot{\epsilon}_f$ depended only weakly on [CS]. After nucleation, we followed the trajectory of the tip of the first propagating crack $r_{\text{tip}}(t)$ (see Fig. S7 in the Supplemental Material [25]), from which we computed the velocity $u_{\text{tip}}$, for different concentrations of particles [CS] as well as different thicknesses, using our MATLAB code (see Fig. 4). We found that the tip propagated with an initial constant velocity $8\,\text{m}\,\text{s}^{-1} < u_{\text{tip}} < 10\,\text{m}\,\text{s}^{-1}$, which is 3 orders of magnitude greater than the velocity of cracks propagating in drying suspensions [31], and slowed down until the maximal extension of the crack was reached. The velocity of the tip was almost an order of magnitude greater than $u_h$, and $u_{\text{tip}}$ remained approximately the same for all particle volume fractions while depending weakly on the thickness of the layer $h$. The fluctuations in velocity of the crack tip at later times for $h = 15 \times 10^{-3}$ m at [CS] = 0.42 (see Fig. 4) seem to be related to a supplementary opening of the crack because of crack widening. A decrease in the release height led to a decrease in the initial velocity (see the inset in Fig. 4). The observations reported in Figs. 2–4 suggest that solidification of the suspensions under large stresses created an elastic material whose properties do not depend on the initial particle volume fraction for the range of [CS] we investigated. We also note that the crack tip velocity has the same order of magnitude as the velocity of the solidification front, $v_{\text{front}} = (\bar{d}/\delta)U$ [22], with $\delta \simeq 6\ \mu$m the interstitial spacing between the particle surfaces (estimated from the particle volume fraction and the average size of the particles assuming they are spherical) and $U = \sqrt{2gH}$ the velocity of the rod at impact.

The elastic properties of the fractured material can be estimated from the magnitude of $u_{\text{tip}}$. For brittle solids, fracture after an impact is a catastrophic process, during which cracks propagate at velocities that are a significant fraction of the velocity of Rayleigh waves $c_R = Ac_s$, with $A \simeq 0.9$ for Poisson ratios $0 < \nu < 0.5$, $c_s = \sqrt{\frac{G}{\rho}}$ the velocity of shear waves, and $G$ the shear modulus of the material [2,32]. We use the relation between the velocity of the crack tip and the velocities of Rayleigh and shear waves to estimate a lower limit for the effective shear modulus $G$ of the fractured material. Knowing the density of our suspensions, $\rho = 1\,590\ \text{kg}\,\text{m}^{-3}$, we equate $c_s$ with $u_{\text{tip}}$ in the definition of $c_s$, and we find $G > \rho u_{\text{tip}}^2 = 8 \times 10^4$ Pa. This lower limit for $G$ is much greater than the storage modulus $G'$ measured during oscillatory shear tests with a rheometer [33]. The latter were performed under the assumption of linear viscoelasticity, which is not valid for the rapid and large strains $\epsilon \simeq 0.12$ we measured (see the inset in

Fig. 3, and Fig. S7 in the Supplemental Material [25]). Our effective value of $G$ should be compared to the value of the shear modulus extracted from large-amplitude oscillatory shear tests, which is a topic of current research [34]. Our estimate does not account for the occurrence of strain hardening [15] and the possible enhancement of fracture due to the reflection of stress waves at the boundaries of the layer.

In conclusion, we have described the response of thin layers of suspensions of non-Brownian particles to an impact. These complex fluids undergo a fluid-to-solid transition and then experience mode-1 fracture accompanied by plastic flow. The number of cracks per impact and their size depend mostly on the thickness of the layer and the particle volume fraction, and only weakly on the energy delivered by the projectile, which is shown to be much higher than the surface energy of the cracks. The conditions for crack nucleation and the velocity at which the cracks propagate suggest that suspensions experiencing large stresses rapidly form a material whose properties depend only weakly on the initial particle volume fraction, over the range of concentrations we probed. We have also given a lower limit for the shear modulus of the fractured material, which we found to be much greater than values reported in the literature for the storage modulus measured in oscillatory shear experiments. We believe this discrepancy is related to the difference in the amplitude and the rate at which the suspensions are deformed in our experiments compared to those typically used in small amplitude oscillatory shear tests. This work opens questions regarding the fracture mechanics of suspensions reported under various conditions [12,15,16] and how it relates to the fluid mechanics of the solvent in the porous material formed by the grains, as well as to the mechanics of wet granular media (i.e., particles in the presence of a very small amount of solvent), in which fracture has also been reported [35,36].

We acknowledge Matteo Ciccotti for fruitful discussions. We acknowledge support from the National Science Foundation through Grant No. CBET-1234500.

[1] B. R. Lawn and T. R. Wilshaw, *Fracture of Brittle Solids* (Cambridge University Press, Cambridge, England, 1993).
[2] K. Ravi-Chandar. *Dynamic Fracture* (Elsevier, New York, 2004).
[3] J. C. Fisher, J. Appl. Phys. **19**, 1062 (1948).
[4] D. D. Joseph, J. Fluid Mech. **366**, 367 (1998).
[5] R. G. Larson, *The Structure and Rheology of Complex Fluids* (Oxford University, New York, 1999).
[6] J. F. Hutton, Nature (London) **200**, 646 (1963).
[7] A. Y. Malkin and C. J. S. Petrie, J. Rheol. **41**, 1 (1997).
[8] J. F. Berret and Y. Séréro, Phys. Rev. Lett. **87**, 048303 (2001).
[9] H. Tabuteau, S. Mora, G. Porte, M. Abkarian, and C. Ligoure, Phys. Rev. Lett. **102**, 155501 (2009).
[10] H. Tabuteau, S. Mora, M. Ciccotti, C.-Y. Hui, and C. Ligoure, Soft Matter **7**, 9474 (2011).
[11] J. R. Gladden and A. Belmonte, Phys. Rev. Lett. **98**, 224501 (2007).
[12] J. M. Schleier-Smith and H. A. Stone, Phys. Rev. Lett. **86**, 3016 (2001).
[13] E. R. Dufresne, E. I. Corwin, N. A. Greenblatt, J. Ashmore, D. Y. Wang, A. D. Dinsmore, J. X. Cheng, X. S. Xie, J. W. Hutchinson, and D. A. Weitz, Phys. Rev. Lett. **91**, 224501 (2003).
[14] M. E. Cates, M. D. Haw, and C. B. Holmes, J. Phys. Condens. Matter **17**, S2517 (2005).
[15] E. E. B. White, M. Chellamuthu, and J. P. Rothstein, Rheol. Acta **49**, 119 (2010).
[16] M. I. Smith, R. Besseling, M. E. Cates, and V. Bertola, Nat. Commun. **1**, 114 (2010).
[17] G. L. Hunter and E. R. Weeks, Rep. Prog. Phys. **75**, 066501 (2012).
[18] A. Fall, N. Huang, F. Bertrand, G. Ovarlez, and D. Bonn, Phys. Rev. Lett. **100**, 018301 (2008).
[19] E. Brown and H. M. Jaeger, Phys. Rev. Lett. **103**, 086001 (2009).
[20] A. Fall, A. Lemaitre, F. Bertrand, D. Bonn, and G. Ovarlez, Phys. Rev. Lett. **105**, 268303 (2010).
[21] M. Roché, H. Kellay, and H. A. Stone, Phys. Rev. Lett. **107**, 134503 (2011).
[22] S. R. Waitukaitis and H. M. Jaeger, Nature (London) **487**, 205 (2012).
[23] R. J. Larsen, J. W. Kim, C. F. Zukoski, and D. A. Weitz, Phys. Rev. E **81**, 011502 (2010).
[24] F. S. Merkt, R. D. Deegan, D. I. Goldman, E. C. Rericha, and H. L. Swinney, Phys. Rev. Lett. **92**, 184501 (2004).
[25] See Supplemental Material at http://link.aps.org/supplemental/10.1103/PhysRevLett.110.148304 for movies of typical impact experiments, information on the rheological response of the suspensions, supplementary information on the dependence of the properties of the crack pattern with the shape and size of the projectile as well as the release height, raw data for Figs. 3 and 4, and a discussion regarding the non-linearity of the viscoelastic regime displayed by the suspensions.
[26] A. G. Evans, M. E. Gulden, and M. Rosenblatt, Proc. R. Soc. A **361**, 343 (1978).
[27] E. M. Morozov. in *Fracture: A Topical Encyclopedia of Current Knowledge*, edited by G. P. Cherepanov (Krieger Pub. Co., Malabar, Florida, 1998), Chap. 22, pp. 440–449.
[28] R. Vermorel, N. Vandenberghe, and E. Villermaux, Phys. Rev. Lett. **104**, 175502 (2010).
[29] Z. P. Bažant, Int. J. Solids Struct. **37**, 69 (2000).
[30] B. Epps, T. T. Truscott, and A. H. Techet, Mathematical Methods in Engineering International Symposium, Coimbra, Portugal, 2010, p. 29.
[31] E. R. Dufresne, D. J. Stark, N. A. Greenblatt, J. X. Cheng, J. W. Hutchinson, L. Mahadevan, and D. A. Weitz, Langmuir **22**, 7144 (2006).
[32] K. F. Graff, *Wave Motion in Elastic Solids* (Dover, New York, 1991).
[33] A. Fall, F. Bertrand, G. Ovarlez, and D. Bonn, J. Rheol. **56**, 575 (2012).
[34] K. Hyun, M. Wilhelm, C. O. Klein, K. S. Cho, J. G. Nam, K. H. Ahn, S. J. Lee, R. H. Ewoldt, and G. H. McKinley, Prog. Polym. Sci. **36**, 1697 (2011).
[35] H. Alarcón, O. Ramos, L. Vanel, F. Vittoz, F. Melo, and J. C. Géminard, Phys. Rev. Lett. **105**, 208001 (2010).
[36] J. C. Géminard, L. Champougny, P. Lidon, and F. Melo, Phys. Rev. E **85**, 012301 (2012).